Int. J. Heat Mass Transfer. Vol. 23, pp. 283–292

0017-9310/80/0301-0283 $02.00/0

SOLID–LIQUID PHASE-CHANGE HEAT TRANSFER AND INTERFACE MOTION IN MATERIALS COOLED OR HEATED FROM ABOVE OR BELOW

N. W. HALE, JR.* and R. VISKANTA

Heat Transfer Laboratory, School of Mechanical Engineering,
Purdue University, West Lafayette, IN 47907, U.S.A.

(*Received* 21 *March* 1979 *and in revised form* 20 *July* 1979)

Abstract – Solid–liquid phase-change heat transfer has been studied experimentally and analytically in several different materials (e.g. stearic acid, sodium phosphate dodecahydrate, sodium sulfate decahydrate and *n*-octadecane) which have been suggested as candidates for latent-heat-of-fusion thermal energy storage materials. Solid–liquid interface motion during freezing and melting from above as well as below has been determined in a rectangular test cell suitable for photographic observations. Comparison of experimental data for *n*-octadecane with predictions based on Neumann and other analyses which account for natural convection heat transfer at the solid–liquid interface show that natural convection in the liquid must be accounted in the prediction of phase-change boundary motion for unstable situations which arise during melting from below and solidification from above.

NOMENCLATURE

A, parameter in equation (43) defined as $(C/H)Ra^m Pr^n$;
c, specific heat;
Fo, Fourier number, $\alpha t/H^2$;
H, height of test cell;
h, heat transfer coefficient;
Δh_f, latent heat of fusion;
k, thermal conductivity;
Nu, Nusselt number defined as hs/k_l;
Pr, Prandtl number, $\mu_l c_l/k_l$;
Ra, Rayleigh number, $g\beta\Delta T s^3/\nu\alpha_l$;
Ste_s, Stefan number for solidification, $c_s(T_f - T_w)/\Delta h_f$;
Ste_l, Stefan number for melting, $c_l(T_w - T_f)/\Delta h_f$;
s, melt or solid layer thickness;
s^*, dimensionless melt or solid layer thickness, s/H;
T, temperature;
t, time;
y, distance from cooled or heated boundary.

Greek symbols

α, thermal diffusivity, $k/\rho c$;
β, thermal expansion coefficient;
Γ, dimensionless parameter, $[h(H-s)/k_l]\,[H/(H-s)]\,(k_l/k_s)\cdot[(T_0 - T_f)/(T_f - T_w)]$;
γ, ratio of densities, ρ_l/ρ_s;
Δ, thermal boundary layer thickness;
Θ, dimensionless temperature, $(T - T_f)/(T_w - T_f)$;
λ, constant defined by equation (10) or equation (13);
ν, kinematic viscosity;
ξ, dimensionless distance, y/H;
ρ, density;
τ, dimensionless time, $Ste \cdot Fo$;
ϕ, shape function defined by equation (23).

Subscripts

f, refers to fusion;
l, refers to liquid;
0, refers to initial;
s, refers to solid;
w, refers to wall.

*Presently at NASA Lyndon B. Johnson Space Center, Houston, TX 77058, U.S.A.

INTRODUCTION

HEAT conduction problems involving solid–liquid phase change are of interest in a wide range of technologies and geophysics. The class of problems involving melting and freezing, generally referred to as "moving boundary" problems, have been the subject of numerous theoretical investigations of various degree of complexity and rigor. The methods of solution used in the analysis of heat conduction problems involving phase change included exact, integral, variational, perturbation, purely numerical and other methods. Extensive literature reviews are available [1–3], and the classical Neumann problem is described in various heat conduction books [4]. Experimental studies of transient heat conduction involving solid–liquid phase transformations and effects of buoyancy have been relatively few [5–7].

Density differences between the solid and liquid phases and buoyancy forces produced by density differences due to temperature variations in the liquid may produce convective motions in the liquid. These and other effects such as superheating of the liquid (or subcooling of solid), physical property dependence on temperature have received little theoretical and even much less experimental attention. The purpose of this study was to determine the effect of heat source/sink

orientation on heat transfer and solid–liquid interface motion during phase change. Specifically, melting and freezing from below and above are studied in a rectangular test cell which allows for photographic observation of the phase-change boundary.

The effect of buoyancy on the one-dimensional melting and freezing of water has been studied experimentally and analytically [5–8]. Thomas and Westwater [9] verified the numerical method of Murray and Landis [10] using their experimental data for *n*-octadecane. The model was extended to include natural convection in the liquid by Boger and Westwater [5] and was verified with their data for water. The velocity of the drift due to the density differences of the two phases [1] during melting and freezing was also accounted for in the numerical model [7] and was checked using the data for water. Studies of convective instabilities in the melting of a horizontal ice layer [11, 12] have also been conducted. Unfortunately, the density inversion of water is unique to this substance, and therefore, the results and conclusions about the effects of buoyancy and density changes during phase transformation cannot be generalized. Melting and solidification of paraffins have also been studied in connection with spacecraft thermal control [13, 14] and thermal energy storage [15], but the effect of the heat source/sink orientation on heat transfer and phase change boundary has not received much attention. It is still common practice in analysis of latent-heat-of-fusion thermal energy storage [15–17] to neglect the effects of convection during solid–liquid phase change.

This paper describes a combined experimental and analytical study of heat transfer during melting and solidification from a horizontal plate (e.g. heat source /sink) facing either upward or downward. A number of different experiments using stearic acid, sodium phosphate dodecahydrate, sodium sulfate decahydrate and *n*-octadecane as test substances have been performed. The work was motivated by the need to gain a more complete understanding of heat transfer processes during solid–liquid phase change in connection with latent-heat-of-fusion thermal energy storage systems.

EXPERIMENTS

Test apparatus

The melting and freezing experiments were performed in a rectangular test cell which allowed for photographic observation of the solid–liquid interface motion in the material during phase transformation. The materials chosen for the study were required to have acceptable light transmission for visual observation, e.g. clear liquid phase and a reasonably opaque solid phase to give a sharp definition of the interface.

A schematic diagram of the test apparatus is shown in Fig. 1. The test cell where melting and freezing took place was placed inside a temperature control chamber which was maintained as close to the fusion temperature of the test material as possible without initiating the melting/freezing process. This was accomplished with two heat exchangers which were installed in the chamber through which water from a constant temperature bath was circulated. The two faces of the chamber were made of glass with removable insulation placed on the windows to allow for photographic observation. In turn, the entire chamber was covered with a 5 cm thick removable styrofoam insulation which had to be lifted off in order to photograph the solid–liquid interface position.

Two copper heat exchangers formed the top and bottom walls of the test cell and served as nearly isothermal heat sources. The vertical walls as well as the front and back faces of the cell were made of plexiglass. The inside dimensions of the test cell were 8.9 cm high, by 14.6 cm wide by 2.2 cm deep. The depth of the test cell was purposely made much smaller than the height or the width in order to minimize the nonuniformities in the melting front position perpendicular to the faces of the cell. Provisions were made for filling the test cell with a liquid and to add additional liquid to completely fill the test cell to account for contraction during the initial solidification. Provisions were also made at one end of the test cell to allow for liquid expansion during melting.

Fifteen chromel–alumel thermocouples were installed at different positions in the test cell. The thermocouple wires extending from the measuring junctions were run parallel to the heated surface along a small diameter rod which supported up to three thermocouples. Nine thermocouples were installed in each heat exchanger. Small diameter holes were drilled into the copper block, and the thermocouples were soldered very close to the surface of the heat exchangers.

Test procedure

Care was taken when filling the test cell with the test material to ensure that no bubbles were trapped in the material. This was accomplished by vibrating the cell during the filling with the phase change material and its solidification.

In the melting experiments with the material initially in the solid phase, water near the fusion temperature was circulated through the heater blocks of the test cell and of the chamber, and the material was preheated to as close to the melting temperature as possible. This was done in order to eliminate the initial

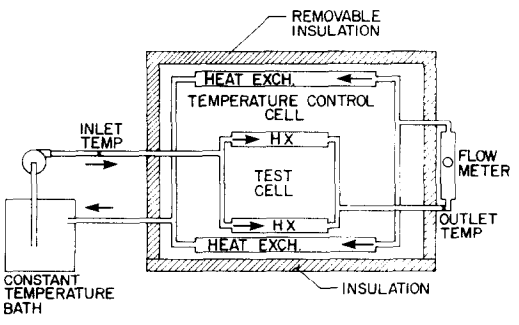

FIG. 1. Schematic diagram of the test arrangement.

subcooling of the solid as one of the parameters which influences the melting. Depending on the particular material being tested, it took from 4 to 18 h to reach the desired conditions. After the material reached a steady, nearly uniform temperature just below its melting point, the temperature of the water circulated through the heater blocks of the test cell was raised to a desired level above the fusion temperature and was maintained there for the duration of the experiment. By closing or opening control valves in the flow circuit the bottom, the top, or both could be heated for a particular test.

At the beginning of each experiment, and at regular intervals thereafter, photographs were taken and other visual observations were made. Photographing and visual observations required that the insulation around the test cell be removed; therefore, these observations were made as rapidly and as infrequently as possible to minimize heat losses from the test cell to the ambient laboratory environment. Thermocouple EMFs and flow meter readings were recorded at the same time.

In freezing experiments, the procedure was similar except that the material was precooled to a uniform temperature just above the fusion temperature before solidification was started. If the experiment was to be melting followed by freezing, as many of them were, there was a period of at least 15 min between the two parts of the experiment when no water was circulated through the heater blocks. This was to allow the constant temperature bath to adjust to the new temperature condition.

ANALYSES

Neumann analysis

Consider first the solidification of a liquid layer which is initially at a uniform temperature T_0. Suddenly at time $t > 0$ the temperature of the boundary at $y = 0$ is lowered to a value T_w which is below the fusion temperature T_f of the material. The physical properties of the two phases are assumed to be different but independent of temperature. The bulk temperature of the liquid at a large distance from the solid–liquid interface is T_0 and constant. This implies that the liquid thickness is effectively infinite, even when it is quite small. If fluid motions due to density differences between the two phases and due to the buoyancy forces in the liquid are neglected [1, 4], the temperature distribution in the solid and liquid phases are governed by the equations

$$\frac{\partial T_s}{\partial t} = \alpha_s \frac{\partial^2 T_s}{\partial y^2}, \quad 0 < y < s(t), \tag{1}$$

$$\frac{\partial T_l}{\partial t} = \alpha_l \frac{\partial^2 T_l}{\partial y^2}, \quad y > s(t), \tag{2}$$

respectively. The initial and boundary conditions are given by

$$T_s(y,0) = T_l(y,0) = T_0 \quad \text{for } t \leq 0, \tag{3}$$

$$T_s(0,t) = T_w \quad \text{for } y = 0 \quad t > 0, \tag{4}$$

$$T_s(s,t) = T_l(s,t) = T_f \quad \text{for } y = s(t), \tag{5}$$

$$T_l(y,t) \to T_0 \quad \text{as } y \to \infty \tag{6}$$

and

$$\rho_s \Delta h_f \frac{ds}{dt} = k_s \left.\frac{\partial T_s}{\partial y}\right|_{y=s} - k_l \left.\frac{\partial T_l}{\partial y}\right|_{y=s} \tag{7}$$

The temperature distribution in the solid phase is given by [4, 18]

$$\Theta_s = 1 - \operatorname{erf}(y/2\sqrt{\alpha_s t})/\operatorname{erf}[(\lambda\gamma)/2\sqrt{\alpha_s}] \tag{8}$$

and in the liquid phase by

$$\Theta_l = 1 - \operatorname{erfc}(y/2\sqrt{\alpha_l t})/\operatorname{erfc}(\lambda/2\sqrt{\alpha_l}). \tag{9}$$

The constant λ is determined from the transcendental equation

$$\frac{1}{Ste_s}\left(\frac{\lambda\gamma}{2}\right) = \sqrt{\frac{\alpha_s}{\pi}}\frac{\exp(-\lambda^2\gamma^2/4\alpha_s)}{\operatorname{erf}(\lambda\gamma/\sqrt{4\alpha_s})} + \sqrt{\frac{\alpha_l}{\pi}}\left(\frac{\rho_l c_l}{\rho_s c_s}\right)\left(\frac{T_0 - T_f}{T_w - T_f}\right)\frac{\exp(-\lambda^2/4\alpha_l)}{\operatorname{erfc}(\lambda/\sqrt{4\alpha_l})} \tag{10}$$

and the solid–liquid interface position is given by

$$s(t) = \lambda\gamma\sqrt{t}. \tag{11}$$

For the melting of a solid the formulation of the problem is similar, and the temperature distribution in the liquid and solid phases is expressed by equations of the same form as equation (9) and (8), respectively. The solid–liquid interface position is given by

$$s = (\lambda/\gamma)\sqrt{t}. \tag{12}$$

The constant λ is determined from the transcendental equation

$$\frac{1}{Ste_l}\left(\frac{\lambda/\gamma}{2}\right) = \sqrt{\frac{\alpha_l}{\pi}}\frac{\exp[-(\lambda/\gamma)^2/4\alpha_l]}{\operatorname{erf}[(\lambda/\gamma)/2\sqrt{\alpha_l}]} + \sqrt{\frac{\alpha_s}{\pi}}\left(\frac{\rho_s c_s}{\rho_l c_l}\right)\left(\frac{T_0 - T_f}{T_w - T_f}\right)\frac{\exp(-\lambda^2/4\alpha_s)}{\operatorname{erfc}(\lambda/2\sqrt{\alpha_s})}. \tag{13}$$

Introduction of the dimensionless time defined as

$$\tau_l = Ste_l \cdot Fo_l = \left[\frac{c_l(T_w - T_f)}{\Delta h_f}\right]\left(\frac{\alpha_l t}{H^2}\right), \tag{14}$$

permits scaling of the Stefan number for the melting problem, for example. Since there is no characteristic length for the one-dimensional diffusion considered here, the height H of the test cell was arbitrarily chosen for the purpose of nondimensionalizing the distance and the Fourier number.

Solidification from above with natural convection at the solid–liquid interface

As long as the system remains stable, the assumption that heat conduction is the only mode of energy transfer and therefore the Stefan analysis is appro-

priate. The onset of instability and development of natural convection in the liquid phase as a result of buoyancy forces due to temperature differences would invalidate the model. Here we present a simple analysis to account for natural convection heat transfer at the solid–liquid interface during solidification from above.

Initially, the liquid temperature T_0 is taken to be above the fusion T_f. Since the solid–liquid interface is colder than the bulk of the liquid, natural convection may develop in the liquid. The temperature distribution in the solid is governed by equation (1), and after the critical Rayleigh number has been exceeded [18] and natural convection develops the temperature distribution in the liquid phase will become and remain uniform at T_0. An energy balance at the solid–liquid interface, equation (7), can then be expressed as

$$\rho_s \Delta h_f \frac{ds}{dt} = k_s \frac{\partial T_s}{\partial y} + h(T_f - T_0) \quad \text{at } y = s(t), \tag{15}$$

where h is the convective heat transfer coefficient available, for example, from correlations [19] for natural convection heat transfer in a fluid confined between two horizontal parallel rigid walls.

In terms of dimensionless variables the governing equation (1) and the initial and boundary conditions can be written as

$$Ste_s \frac{\partial \Theta_s}{\partial \tau_s} = \frac{\partial^2 \Theta_s}{\partial \xi^2} \tag{16}$$

and

$$\Theta_s = \Theta_0 \quad \text{for } \tau < 0 \text{ and any } \xi, \tag{17}$$

$$\Theta_s = 1.0 \quad \text{at } \xi = 0 \text{ and } \tau_s > 0, \tag{18}$$

$$\Theta_s = 0 \quad \text{at } \xi = s^*, \tag{19}$$

$$\frac{ds^*}{d\tau_s} = \frac{\partial \Theta_s}{\partial \xi} - \Gamma \quad \text{at } \xi = s^*. \tag{20}$$

The nonlinearity introduced by the boundary condition, equation (20), precludes a closed form exact analytical solution. The solution of equation (16) with the initial and boundary conditions, equations (17) through (20), can be obtained using numerical [10, 20] perturbation [21, 22] or integral [23] methods. We adopt here an integral method of solution.

As an approximation for the temperature distribution in the solid layer the functional form for $\Theta_s(\xi, \tau_s)$ is postulated in terms of two undetermined functions $s^*(\tau_s)$ and $\phi(\tau_s)$ such that

$$\Theta_s = \phi\left(\frac{\xi}{s^*}\right) + (1 - \phi)\left(\frac{\xi}{s^*}\right)^2. \tag{21}$$

The function $\phi(\tau_s)$ is determined by requiring that $\phi(\tau_s)$ be independent of $ds^*/d\tau_s$ [23]. This can be derived in the following way. By differentiating equation (19) with respect to τ_s, we obtain

$$\frac{\partial \Theta_s}{\partial \xi}\frac{ds^*}{d\tau_s} + \frac{\partial \Theta_s}{\partial \tau_s} = 0. \tag{22}$$

The elimination of $ds^*/d\tau_s$ between equations (20) and (22) and substitution of the resulting equation to eliminate $\partial\Theta_s/\partial\tau_s$ from equation (16) yields the necessary condition for determining $\phi(\tau_s)$

$$\left\{Ste_s\left[\left(\frac{\partial \Theta_s}{\partial \xi}\right)^2 - \Gamma\left(\frac{\partial \Theta_s}{\partial \xi}\right)\right] + \frac{\partial^2 \Theta_s}{\partial \xi^2}\right\}_{\xi = s^*} = 0. \tag{23}$$

Substitution of equation (21) into equation (23) and solution results in

$$(2 - \phi) = [(b - c) + \sqrt{(b - c)^2 + 4c}]/2, \tag{24}$$

where

$$b = \Gamma s^*,$$

$$c = 2/Ste_s.$$

Now with ϕ determined, an energy balance at the phase change interface boundary, equation (20), yields the following differential equation for the interface position $s^*(\tau_s)$

$$\frac{ds^*}{d\tau_s} = \frac{(2 - \phi)}{s^*} - \Gamma \quad \text{at } \xi = s^*. \tag{25}$$

Integration of equation (25) yields

$$\tau_s = \int_0^{s^*} \frac{\eta d\eta}{[(2 - \phi) - \Gamma\eta]}. \tag{26}$$

Unfortunately, this integral cannot be evaluated analytically because both ϕ and Γ depend on s^* in a complicated way.

For the special case of negligible heat capacity in the solid ($Ste_s \to 0$), equation (26) becomes

$$\tau_s = \int_0^{s^*} \frac{\eta d\eta}{(1 - \Gamma\eta)}. \tag{27}$$

In the absence of convection at the solid–liquid interface ($\Gamma = 0$), evaluation of the integral in equation (27) gives

$$s^* = \sqrt{2\tau_s}, \tag{28}$$

if it is assumed that $s^* = 0$ at $\tau_s = 0$.

Melting from below with natural convection in the melt

It has been experimentally observed [8, 12] and theoretically predicted [24] that a convective instability develops in a horizontal melt layer created by a solid-to-liquid phase change. If the Rayleigh number is sufficiently large, natural convection in the melt could significantly affect heat transfer and the interface motion. Here we present a simple analysis to predict the solid–liquid interface position during melting of a solid heated from below.

A solid of sufficient lateral extent so that the edge effects could be neglected is initially at a temperature T_0 below the fusion temperature T_f. At time $t > 0$ heating is initiated at the lower bounding surface ($y = 0$) as a step increase in the wall temperature to a value T_w. During the early stages of the phase-change process when the melt layer is stable, the temperature

distribution and the interface position are predicted by the Neumann analysis. After the critical Rayleigh number, Ra_c, and the corresponding critical time, t_c, have been exceeded, the interface motion is determined by the convective heat transfer to the phase-change boundary. The energy balance at the interface is still valid, but the conductive heat flux in the liquid — $k_l \partial T_l/\partial y$ is replaced by the convective heat flux so that the energy balance at the interface becomes

$$\rho_l \Delta h_f \frac{ds}{dt} = h(T_w - T_f) + k_s \frac{\partial T_s}{\partial y}, \tag{29}$$

where the convective heat transfer coefficient h is available from correlations [19] for natural convection. The temperature distribution in the solid is predicted from the energy equation in the solid, equation (1), with appropriate initial and boundary conditions.

For time $t > t_c$ the temperature distribution in the solid and the phase-change boundary are predicted from the energy equation

$$Ste_s \frac{\partial \Theta_s}{\partial \tau_s} = \frac{\partial^2 \Theta_s}{\partial \xi^2} \quad \text{for } \xi > s^*, \tau > \tau_c \tag{30}$$

and the following initial and boundary conditions:

$$\Theta_s \to \Theta_0 \quad \text{for } \tau_s \to \tau_c \quad \text{and } \xi \to \infty, \tag{31}$$

$$\Theta_s = 1 \quad \text{at } \xi = s^* \tag{32}$$

and

$$s^* \frac{ds^*}{d\tau_l} = s^* \left(\frac{k_s}{k_l}\right) \frac{\partial \Theta_s}{\partial \xi} + Nu \quad \text{at } \xi = s^*. \tag{33}$$

Because of the nonlinearity introduced by the boundary motion, equation (33), an exact, closed-form analytical solution is not possible. Therefore, an approximate solution will be obtained using an integral method [22, 25].

If the energy equation, equation (30), is integrated over the dimensionless thermal boundary layer thickness Δ, there results

$$Ste_s \frac{d}{d\tau_s} \int_{s^*}^{\Delta} \Theta_s d\xi = \left.\frac{\partial \Theta_s}{\partial \xi}\right|_{\Delta} - \left.\frac{\partial \Theta_s}{\partial \xi}\right|_{s^*} - \Theta_s\Big|_{s^*} \frac{ds^*}{d\tau} + \Theta_s\Big|_{\Delta} \frac{d\Delta}{d\tau}. \tag{34}$$

A second order polynomial for the temperature distribution in the solid, e.g.

$$\Theta_s = [(\Delta - \xi)/(\Delta - s^*)]^2, \tag{35}$$

which satisfies the conditions

$$\Theta_s = 1.0 \quad \text{at } \xi = s^*, \tag{36}$$

$$\Theta_s \to 0 \quad \text{as } \xi \to \Delta \tag{37}$$

and

$$\partial \Theta_s/\partial \xi \to 0 \quad \text{as } \xi \to \Delta, \tag{38}$$

is assumed as an approximation of the profile.

Substitution of equation (35) into equation (34) and use of the boundary condition gives

$$\frac{1}{3} Ste_s \frac{d}{d\tau_s}(\Delta - s^*) = \left\{\left(\frac{2}{\Delta - s^*}\right)\left(1 + \frac{k_s}{k_l}\right) - Nu/s^*\right\}. \tag{39}$$

Combining equation (35) with equation (33) yields

$$s^* \frac{ds^*}{d\tau_l} = -\frac{2s^*}{(\Delta - s^*)}\left(\frac{k_s}{k_l}\right) + Nu. \tag{40}$$

Equations (39) and (40) are solved with the initial conditions

$$s^* = s_c^* \quad \text{and } \Delta - s^* = \Delta_c - s_c^* \quad \text{at } \tau = \tau_c, \tag{41}$$

where Δ_c is the initial penetration depth at $\tau_s = \tau_c$ which can be obtained by matching equation (10) with equation (35) at $\tau = \tau_c$.

Depending on the Rayleigh number range, the natural convection heat transfer between two rigid parallel boundaries maintained at different temperatures can be expressed as [19]

$$Nu = \frac{hs}{k_l} = \left(\frac{hH}{k_l}\right)\left(\frac{s}{H}\right) = CRa^m Pr^n = A(s^*)^{3m}, \tag{42}$$

where A is independent of s^*. The constant C and the exponents m and n are different for the creeping, laminar, transition and turbulent regions. For the special case of the solid initially and held at the fusion temperature, the solution of equation (40) is

$$\left(\frac{1}{2 - 3m}\right)(s^{*2-3m} - s_c^{*2-3m}) = A(\tau_l - \tau_c). \tag{43}$$

If $m = 1/2$, equation (42) indicates that the melt layer thickness will increase linearly with time while the Neumann analysis predicts that the melt layer will grow as $\sqrt{\tau_l}$. It should be emphasized, however, that equation (42) has been determined on the basis of steady-state natural convection heat transfer in the absence of phase-change, and therefore use of the equation in a situation where one of the boundaries is moving may not be appropriate.

RESULTS AND DISCUSSION

Qualitative discussion of experimental results

Numerous experiments were performed which yielded valuable qualitative and quantitative data about the solid–liquid interface motion and temperature distribution during solid–liquid phase-change heat transfer in the materials. A detailed discussion of the results is available [26], and thus only a few selected experiments will be highlighted here.

Figure 2 shows a comparison of the interface motion for melting of stearic acid from above and below. The solid was purposely not preheated and its initial temperature was over 40°C below the fusion temperature. The solid–liquid interface velocity is seen to be much larger for melting from below than above. For the latter the interface motion nearly comes to a halt at

times. The differences between the two experiments is attributed to the higher heat transfer due to natural convection which occurs when the material is heated from below but not when the material is heated from above. In experiments where the heating surface was facing upward natural convection set in very rapidly but was never observed when the heating surface faced downward. Natural convection manifested itself in a form of easily observable cells which grew in size as the melt layer thickness increased. The solid–liquid interface was irregular and provided evidence of cellular convection. These observations concur with experimental results for melting of ice from below [6]. During melting from above the interface remained flat, indicating the absence of convection. Furthermore, convection cells were not observed for this arrangement.

Experiments with sodium phosphate dodecahydrate ($Na_2HPO_4 \cdot 12H_2O$, $T_f = 36°C$) revealed that the material began to break down with the first melting/freezing cycle and stratified into various layers: anhydride, different hydrates (believed to be $Na_2HPO_4 \cdot 12H_2O$, $Na_2HOP_4 \cdot 7H_2O$, $Na_2HPO_4 \cdot 5H_2O$, etc. but no chemical analysis was made), and water. In addition, observations indicated that water was trapped in some of the crystal layers, making the layers inhomogeneous. For example, a short time after the second melting cycle was started the layers were: solid anhydride, liquid hydrate, dodecahydrate crystals, heptahydrate crystals and water. After the underlying dodecahydrate crystal layer had melted the heptahydrate crystal layer fell to the bottom of the test cell and mixed with the liquid. This type of unpredictable behavior made it very difficult to interpret the results quantitatively. The test cell and the experimental procedure were not designed to study bulk motion of the solid hydrate crystal layer after it had lost support at the cell walls.

In the first experiment with sodium sulfate decahydrate ($NaSO_4 \cdot 10H_2O$; $T_f = 32.4°C$), the hydrate was completely solid before heating from below was started. However, as the melting proceeded, anhydride was deposited at the bottom of the test cell. When the cell was cooled only a small fraction of the material resolidified as a salt hydrate complex. The material was heated and upon cooling and stirring a large portion of the material did form as crystals but a layer of water remained on the top. However, after remelting there was again a layer of solid material deposited on the bottom of the test cell. And after the material had been cooled below the fusion temperature, only a very small crystal layer formed. Nucleating and thickening agents have been recommended [27] to aid nucleation and prevent segregation of a Glauber's salt. Upon addition of sodium tetraborate (borax) only about 25% of the salt hydrate formed crystals, and these crystals were inhomogeneous mixed with water.

In the next two subsections the experimental results obtained for *n*-octadecane (99% pure) will be compared with analytical predictions because the physical and transport properties are well established [28] to make such a comparison meaningful. The physical and transport properties of *n*-octadecane used in the data reduction were taken from Ref. [29]. For stearic acid the transport property data are incomplete. No comparisons of experimental data obtained for sodium phosphate dodecahydrate and sodium sulfate decahydrate are possible with analysis because of the nonhomogeneous structure of the materials as a result of segregation of the hydrates into anhydrous salts and water, bulk motion of the crystals during melting and unpredictable as well as unrepeatable behavior during phase change. Despite the promise that the salt hydrates have for low temperature latent heat thermal energy storage, the experience with these materials indicate it will be difficult to predict the system performance due to their complex behavior during cyclic melting and freezing.

Heat transfer under stable conditions

When a liquid is cooled from below or a solid is heated from above, the fluid layer is stable, and the Neumann model for one-dimensional phase-change heat transfer should be appropriate. Figure 3 shows a

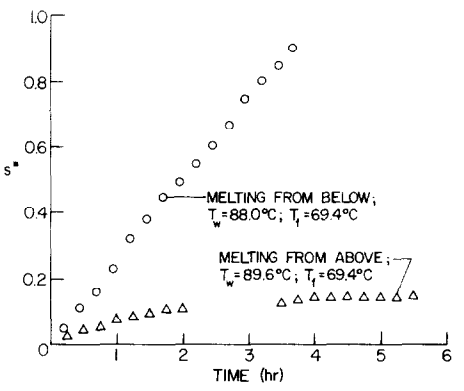

FIG. 2. Variation of solid–liquid interface position with time during melting of stearic acid from above and below.

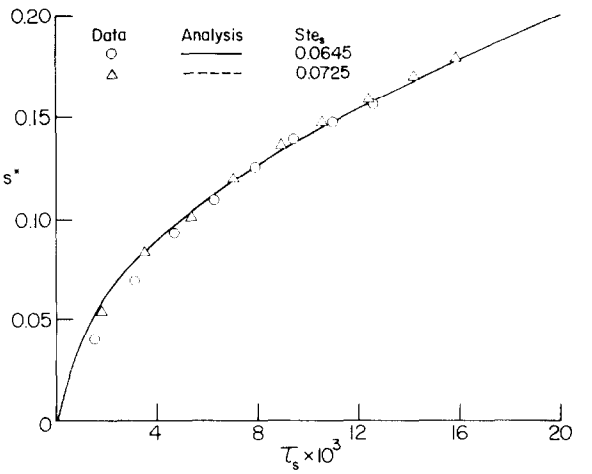

FIG. 3. Comparison of measured and predicted (Neumann model) solid–liquid interface positions during solidification of *n*-octadecane from below: (a) $Ste_s = 0.0645$ ($T_w = 20.2°C$) and (b) $Ste_s = 0.0725$ ($T_w = 19.3°C$).

comparison of the solid–liquid interface position predicted from the Neumann analysis with experimental data during solidification. For $Ste_s = 0.0725$ the analysis predicts the phase-change boundary which overlaps the curve for $Ste_s = 0.0645$ and separate lines could not be drawn. At early times ($\tau_s < 0.004$) the analysis predicts a faster rate of solidification than experimentally observed, but at later times there is good agreement between predictions and data. A comparison of the predicted temperature variation with experimental data at a few selected locations is given in Fig. 4. Again, there is substantial agreement between the two results. An increase in interfacial velocity was obtained for solidification of *n*-hexadecane at later time [14]. This was attributed to the departure from one-dimensional analysis and the neglect of heat gain from the environment as the interface approached a cooled top plate.

The predicted and measured solid–liquid interface positions for melting from above are compared in Fig. 5. Separate curves could not be clearly drawn for the two Stefan numbers. The agreement between data and analysis is reasonably good for early times ($\tau_l < 0.008$),

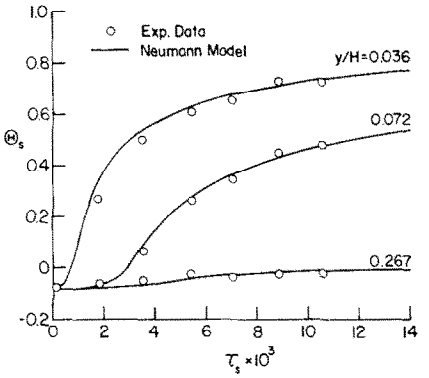

FIG. 4. Comparison of measured and predicted temperature distributions during solidification of *n*-octadecane from below: $Ste_s = 0.0725$ ($T_w = 20.2$°C).

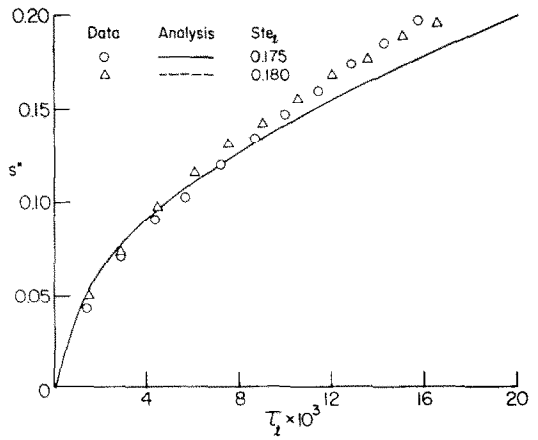

FIG. 5. Comparison of measured and predicted (Neumann model) solid–liquid interface positions for melting of *n*-octadecane from above: (a) $Ste_l = 0.175$ ($T_w = 43.4$°C) and (b) $Ste_s = 0.180$ ($T_w = 44.0$°C).

but at later times the observed melt layer thickness was greater than that predicted. The fluid motion due to the density differences of the two phases could possibly account for part of the discrepancy, but this effect is expected to be relatively small [7, 30]. The primary reason for the discrepancy between data and predictions at later time ($\tau_l > 0.008$) is believed to be due to weak natural convection which developed as a result of heat conduction along the vertical test cell walls.

Heat transfer under unstable conditions

A comparison of the experimental data with predictions based on the Neumann analysis shows that for $Ste_s = 0.0354$ the data are in general somewhat lower than the predictions, see Fig. 6. Note also that for this case the interface position predicted by the convection model is less than 2% lower than the Stefan model because heat transfer by convection is not significant. The agreement between the data and predictions is reasonably good because the initial liquid temperature was close to the fusion temperature so that the Rayleigh number at $\tau_s = 0$ was relatively small ($Ra \simeq 2.5 \times 10^6$) and decreased as the cooling continued. However, for the higher Stefan number ($Ste_s = 0.0734$) the data are as much as 30% lower than the Neumann analysis at $\tau_s = 0.012$ (dashed curve is not shown for clarity because it is very close to the curve for $Ste_s = 0.0354$). The discrepancy between the two results is due to the natural convection in the liquid. For this case the Rayleigh number, based on the depth of the liquid layer, at the start of the cooling was about 3×10^7 even though the initial liquid temperature was only about 1°C higher than the fusion temperature. The results clearly show that for an accurate prediction of the solid–liquid interface position the effects of natural convection in the liquid must be considered when solidification takes place from above.

As already discussed, natural convection develops

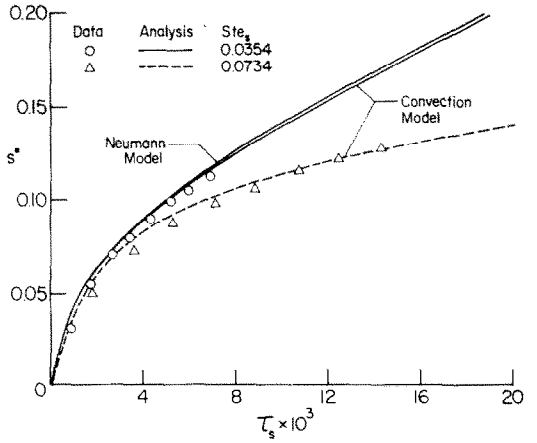

FIG. 6. Comparison of measured phase-change boundary positions with predictions for solidification of *n*-octadecane from above: (a) $Ste_s = 0.0354$ ($T_w = 23.5$°C) and (b) $Ste_s = 0.0734$ ($T_w = 19.2$°C).

when the test material is melted from below, and it is estimated that for $Ste_l = 0.128$ the critical Rayleigh number ($\simeq 1700$) [24] is reached when the melt layer becomes about 1.6 mm thick or $s^* \simeq 0.02$. Figure 7 shows that the Neumann analysis (only one curve is drawn because the others are too close to be clearly indicated) greatly under-predicts the rate of melting. The simple convection model [equations (39) and (40)] over-predicts the rate of melting, but is in a much better agreement with the data. One reason for the discrepancy is the inadequacy of the model itself. Another reason may be due to the natural convection heat transfer correlations [19] used which were developed from data obtained under steady state, no phase-change conditions. Other correlations are available (see Chu and Goldstein [31] for a more complete list of relevant references) and could have been used in the calculations. The semi-empirical correlations of O'Toole and Silveston [19] were used because data for high Prandtl number fluids were employed in developing the equations and were therefore chosen for this reason. For example, the Prandtl number of *n*-octadecane near its fusion temperature is about 68.

The temperature history of *n*-octadecane during heating from below is presented in Fig. 8. Comparison of Figs. 7 and 8 clearly shows that once melting has occurred natural convection develops rapidly. As evidence of this, note the sharp rise in the temperature of the liquid. Also, except for the two boundary layers at the heated wall and the solid–liquid interface, the rest of the melt layer is practically isothermal. The temperature of the liquid, however, increases with time as the heating is continued. The data for this particular and other experiments show that the melt temperature near the heated bottom wall reaches a maximum and then decreases. These trends in temperature–time history can be attributed to changes from pseudo-conduction through transition to fully developed natural convection during the melting process [28].

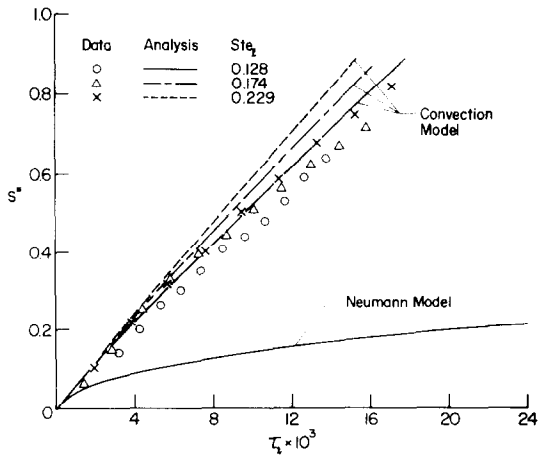

FIG. 7. Comparison of measured phase-change boundary positions with predictions for melting of *n*-octadecane from below: (a) $Ste_l = 0.128$ ($T_w = 39.2°C$); (b) $Ste_l = 0.174$ ($T_w = 32.4°C$) and (c) $Ste_l = 0.229$ ($T_w = 48.5°C$).

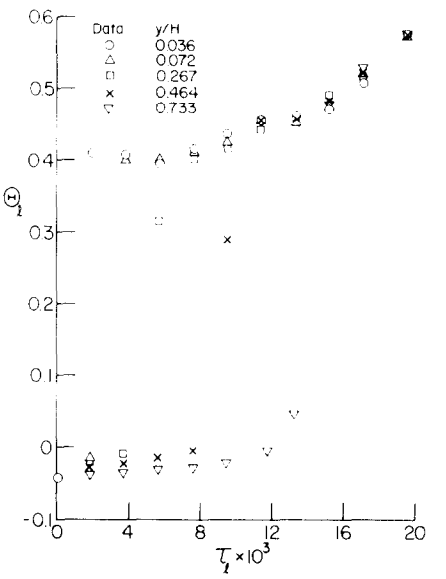

FIG. 8. Temperature distribution during melting of *n*-octadecane from below: $Ste_l = 0.229$ ($T_w = 48.5°C$).

The results of the present work are supported by the findings of other investigators for melting of *n*-paraffins [9, 13, 29]. For example, the measured interfacial velocities during melting of *n*-octadecane exceeded analytical predictions by as much as 100%, and the difference was attributed to irregularities at interface [9]. The continuous replacement of an effective thermal conductivity of the liquid, which was calculated from $k_{eff.l} \equiv Nu \times k_l$, resulted in improved agreement of the interface position data with calculations [26, 29]. However, this scheme is conceptually questionable and would not be expected to yield true temperatures in the liquid because convection would arbitrarily be replaced by conduction in a hypothetical medium with a larger, time dependent thermal conductivity than that of the liquid.

CONCLUDING SUMMARY

The results obtained for one dimensional, solid–liquid phase-change heat transfer under stable conditions, e.g. melting from a downward facing wall and freezing from an upward facing wall, agree within the experimental accuracy to the predictions based on the Neumann analysis.

In the unstable situation of freezing from above natural convection at the solid–liquid interface may decrease the rate of solidification at later times if the Rayleigh number is sufficiently large. When melting from below natural convection develops rapidly and greatly influences heat transfer and the motion of the phase-change boundary during the process. The approximate analyses which take into account natural convection in the liquid under unstable situations yield reasonably good agreement with the data but are not completely satisfactory and more fundamental approaches are required.

The findings of this study demonstrate the impor-

tance of natural convection in solid–liquid phase-change heat transfer under unstable conditions. The practice [3, 15–17, 32, 33], for example, of neglecting the effects in the analysis of such problems does not appear reasonable. Natural convection has to be considered in the analysis of unstable phase-change processes if good agreement between data and predictions for the solid–liquid interface position is to be obtained.

Acknowledgements — The work described in this paper was supported by the National Science Foundation Heat Transfer Program under Grant Nos. ENG 75-15030 and ENG 78-11686. The authors wish to acknowledge the assistance of Mr. K.-H. Lee in computer programming and data reduction.

REFERENCES

1. S. G. Bankoff, Heat conduction and diffusion with a phase change, in *Advances in Chemical Engineering*, edited by T. B. Drew, *et al.*, Vol. 5, pp. 75–150. Academic Press, New York (1964).
2. L. I. Rubinshtein, *The Stefan Problem*. American Mathematical Society, Providence, RI (1971).
3. D. G. Wilson, A. D. Solomon and P. T. Boggs, Editors, *Moving Boundary Problems*. Academic Press, New York (1978).
4. H. S. Carslaw and J. C. Jaeger, *Conduction of Heat in Solids*, 2nd Ed., pp. 283–296. Oxford University Press, New York (1959).
5. D. V. Boger and J. W. Westwater, Effect of buoyancy on the melting and freezing process, *Trans. ASME, Ser. C, J. Heat Transfer* **89**, 81–89 (1967).
6. W. L. Heitz and J. W. Westwater, Critical Rayleigh numbers for natural convection of water confined in square cells with L/D from 0.5 to 8, *Trans. ASME, Ser. C, J. Heat Transfer* **93**, 188–196 (1971).
7. W. L. Heitz and J. W. Westwater, Extension of the numerical method for melting and freezing problems, *Int. J. Heat Mass Transfer* **13**, 1371–1375 (1970).
8. Y. C. Yen and F. Galea, Onset of convection in a layer of water formed by melting of ice from below, *Phys. Fluids* **11**, 1263–1269 (1968).
9. J. C. Thomas and J. W. Westwater, Microscopic study of solid–liquid interfaces during melting and freezing, *AIChE Chem. Eng. Prog. Symp. Ser.* **59**(41), 155–164 (1963).
10. W. D. Murray and F. Landis, Numerical and machine solutions of transient heat conduction problems involving phase change, *Trans. ASME, Ser. C, J. Heat Transfer* **81**, 106–112 (1959).
11. S. Martin and P. Kauffman, The evolution of the under-ice melt ponds, or double diffusion at freezing point, *J. Fluid Mech.* **64**, 507–527 (1974).
12. N. Seki, S. Fukosako and M. Sugawara, A criteria on onset of free convection in a horizontal melted water layer with free surface, *Trans. ASME, Ser. C, J. Heat Transfer* **99**, 92–98 (1977).
13. P. R. Pujudo, J. F. Stermole and J. O. Golden, Melting of a finite paraffin slab as applied to phase change thermal control, *J. Spacecraft Rockets* **6**, 280–284 (1969).
14. A. D. Ukanawa, F. J. Stermole and J. O. Golden, Phase change solidification dynamics, *J. Spacecraft Rockets* **8**, 193–196 (1971).
15. J. A. Bailey, C.-K. Liao, S. I. Güceri and J. C. Mulligan, A solar energy storage subsystem utilizing the latent heat of fusion paraffin hydrocarbons — a progress report, in *Proc. Workshop on the Solar Energy Storage Subsystems for the Heating and Cooling of Buildings*, ASHRAE, Cleveland, pp. 75–84 (1975).
16. J. Meakin, J. Stuchlik and F. A. Costello, Coolness storage in a sodium sulfate decahydrate mixture, ASME Paper No. 76-WA/HT-35 (1976).
17. D. J. Morrison and S. U. Abdel-Khalik, Effects of phase change energy storage on the performance of air based and liquid based solar heat of fusion systems, *Solar Energy* **20**, 57–67 (1978).
18. E. R. F. Eckert and R. M. Drake, *Analysis of Heat and Mass Transfer*, pp. 224–228. McGraw-Hill, New York (1972).
19. J. L. O'Toole and P. L. Silveston, Correlations of convective heat transfer confined in horizontal layers, *AIChE Chem. Eng. Prog. Symp. Ser.* **32**(57), 81–86 (1961).
20. J. S. Goodling and M. S. Khader, Results of the numerical solution for outward solidification with heat flux boundary conditions, *Trans. ASME, Ser. C, J. Heat Transfer* **97**, 307–309 (1975).
21. F. Megerlin, Geometrisch eindimensionale Wärmeleitung beim Schmelzen und Erstarren, *Forsch. Ing.-Wes.* **34**, 40–46 (1968).
22. K. Stephan and B. Holzknecht, Die Asymptotischen Lösungen für Vorgänge des Erstarrens, *Int. J. Heat Mass Transfer* **19**, 597–1602 (1976).
23. T. R. Goodman, Application of integral methods to transient nonlinear heat transfer, in *Advances in Heat Transfer*, edited by T. F. Irvine, Jr. and J. P. Hartnett, Academic Press, New York. Vol. 1, pp. 51–122 (1964).
24. E. M. Sparrow, L. Lee and N. Shamsundar, Convective instability in a melt layer heated from below, *Trans. ASME, Ser. C, J. Heat Transfer* **98**, 88–94 (1976).
25. C. Tien and Y.-C. Yen, Approximate solution of a melting problem with natural convection, *AIChE Chem. Eng. Prog. Symp. Ser.* **62**(64), 166–172 (1966).
26. N. W. Hale, Jr., Heat transfer during melting and freezing of phase change thermal energy storage materials, M.S. Thesis, Purdue University, August (1978).
27. M. Telkes, Solar energy storage, *ASHRAE J.* **9**, 38–44 (1974).
28. A. G. Bathelt, R. Viskanta and W. Leidenfrost, An experimental investigation of natural convection in the melted region around a heated horizontal cylinder, *J. Fluid Mech.* **90**, 227–239 (1979).
29. W. R. Humphries and E. I. Griggs, A design handbook for phase change thermal control and energy storage devices, NASA Technical Paper 1074, Washington, DC (1977).
30. B. W. Grange, R. Viskanta and W. H. Stevenson, Diffusion of heat and solute during freezing of salt solutions, *Int. J. Heat Mass Transfer* **19**, 373–384 (1976).
31. F. Y. Chu and R. J. Goldstein, Turbulent convection in a horizontal layer of water, *J. Fluid Mech.* **60**, 141–159 (1973).
32. S. Kumar and F. A. Costello, The design of a sodium sulfate decahydrate heat exchanger for coolness storage, in *Proc. 12th Intersociety Energy Conversion Conference*, American Nuclear Society, LaGrange, Illinois, pp. 511–516 (1977).
33. L. G. Marianowski and H. C. Maru, Latent heat thermal energy storage systems above 450°C, in *Proc. 12th Intersociety Energy Conversion Conference*, American Nuclear Society, LaGrange, Illinois, pp. 555–566 (1977).

TRANSFERT THERMIQUE ASSOCIE AU CHANGEMENT DE PHASE SOLIDE–LIQUIDE ET MOUVEMENT D'INTERFACE DANS DES MATERIAUX REFROIDIS OU CHAUFFES PAR DESSUS OU PAR DESSOUS

Résumé — On étudie expérimentalement et analytiquement le transfert thermique associé ou changement de phase solide–liquide, dans différents matériaux qui ont été considérés comme susceptibles d'être utilisés dans le stockage d'énergie thermique. On détermine le mouvement de l'interface solide–liquide pendant le refroidissement et la fusion, aussi bien par dessus que par dessous, dans une cellule rectangulaire permettant des observations photographiques. La comparaison entre expérience pour le *n*-octadécane et le calcul selon Neumann et autres analyses qui tiennent compte de la convection naturelle à l'interface, montre que la convection naturelle dans le liquide doit être considérée dans la prévision du mouvement de la frontière pour les situations instables qui apparaissent pendant la fusion à partir du bas et le solidification à partir du haut.

WÄRMEÜBERGANG UND GRENZFLÄCHENBEWEGUNG BEI DER PHASENÄNDERUNG FLÜSSIG-FEST IN VON OBEN ODER UNTEN GEKÜHLTEN ODER ERWÄRMTEN STOFFEN

Zusammenfassung — Der Wärmeübergang bei der Phasenänderung flüssig–fest wurde experimentell und analytisch für verschiedene Stoffe untersucht, die als Latentwärmespeicher-Materialien vorgeschlagen wurden. Die Bewegung der Phasengrenzfläche während des Gefrierens und Schmelzens sowohl von oben als auch von unten wurde in einer rechteckigen Testzelle, die für fotografische Beobachtungen eingerichtet war, bestimmt. Ein Vergleich von Versuchergebnissen für *n*-Oktadekane mit Berechnungen, die sich auf analytische Betrachtungen von Neumann und anderen stützen und den Wärmeübergang bei natürlicher Konvektion an der Phasengrenzfläche fest–flüssig berücksichtigen, zeigt, daß die natürliche Konvektion in der Flüssigkeit berücksichtigt werden muß, um Phasengrenzflächenbewegung für labile Lagen, die sich während des Schmelzens von unten und des Erstarrens von oben einstellen, voraussagen zu können.

ТЕПЛОПЕРЕНОС МЕЖДУ ТВЕРДЫМ ТЕЛОМ И ЖИДКОСТЬЮ ПРИ ФАЗОВЫХ ПРЕВРАЩЕНИЯХ И ПЕРЕМЕЩЕНИЕ ПОВЕРХНОСТИ РАЗДЕЛА В МАТЕРИАЛАХ, ОХЛАЖДАЕМЫХ ИЛИ НАГРЕВАЕМЫХ СВЕРХУ ИЛИ СНИЗУ

Аннотация — Экспериментально и теоретически исследовался теплоперенос между твердым телом и жидкостью при фазовых превращениях на ряде различных материалов (например, стеариновая кислота, додекагидрат фосфата натрия, декагидрат сульфата натрия и *n*-октадекан), предложенных для возможного использования в качестве материалов, аккумулирующих скрытую тепловую энергию фазового перехода. Наблюдение за перемещением поверхности раздела между твердым телом и жидкостью во время затвердевания или плавления как сверху, так и снизу осуществлялось в прямоугольной экспериментальной ячейке, позволяющей проводить фотографирование процесса. Сравнение экспериментальных данных по *n*-октадекану с результатами расчётов по методу Ноймана и другим методам, которые учитывают теплообмен естественной конвекцией на границе раздела фаз, показывает, что при рассмотрении перемещения границы фазового перехода в неустойчивых ситуациях, наблюдаемых при плавлении снизу или затвердевании сверху, необходимо учитывать естественную конвекцию в жидкости.